Inertial active particles in a Poiseuille flow: negative mobility and particle separation

Ankit Gupta^{1,*} and P. S. Burada^{1,†}

¹Department of Physics, Indian Institute of Technology Kharagpur, Kharagpur 721302, India (Dated: November 19, 2025)

The diffusive behavior of small entities is strongly influenced by the flow of the surrounding medium, which is ubiquitous in natural and artificial environments. In this study, we investigate the transport characteristics of the inertial active Brownian particles (ABPs) in a microfluidic channel under a Poiseuille flow. The interplay between the inertia of the particles and the imposed fluid flow leads to interesting diffusive behaviors. For instance, in the overdamped regime $(m \to 0)$, particles exhibit a negative average velocity $\langle v \rangle$ due to upstream movement. As m increases, particles tend to move along the flow direction with an increase in $\langle v \rangle$ in the positive direction, exhibiting a maximum at optimal m, and diminish for higher m values. The effective diffusion coefficient D_{eff} also shows a peak at this optimal m. Interestingly, at higher m values, D_{eff} decreases with increasing the noise strength. The self-propelled velocity of the particles further enhances the upstream movement. Further, the rotation rate of the particles also contributes positively to the upstream motion, and enhances the diffusion of the particles by many orders in the limit of higher m. This study reveals that inertia not only modifies swimmer-flow interactions but also enables new dynamical regimes, where mass-dependent trajectories can be harnessed for selective control. Such control holds promise for mass-based particle separation in precisely engineered environments and lab-on-a-chip devices for technological applications.

I. INTRODUCTION

The Microorganisms or the artificial swimmers, while swimming in a complex fluid under the geometrical constraints, often lead to interesting transport phenomena [1–5]. The study of such systems has revealed behaviors absent in passive particles, e.g., persistent swimming, accumulation near the boundaries, collective pattern formation, and non-equilibrium phase transitions [2, 5–7]. Unlike passive particles, which move only under external forces, ABPs generate their own propulsion through internal energy conversion, as seen in bacterial suspensions [8–10] and engineered microswimmers, i.e., self-propelled colloids [11, 12].

The collective dynamics of ABPs in shear flow are of fundamental importance across natural and engineered environments, from open oceans to narrow capillaries [5, 13]. Microswimmers such as bacteria, sperm cells, and other microorganisms often navigate through confined spaces under the influence of background flows, as seen in pathogen transport in lung mucus [14], microbial motion through porous media [15], sperm motility in the female reproductive tract [16], and blood cell transport through the vascular system [17]. Artificial microswimmers—including colloids and microrobots—are likewise designed to function in structured, flowing environments with applications in drug delivery [18], water remediation [19, 20], particle separation [21, 22], and disease diagnosis [23]. Most studies, however, focus on the low-Reynolds-number regime where inertia is negligible, revealing phenomena such as wall accumulation [24, 25] and upstream swimming in Poiseuille flow [25, 26]. By contrast, much less is known about the inertial regime, where viscosity and inertia compete, leading to qualitatively new behaviors such as negative mobility and mass-based particle separation.

In recent years, experimental and theoretical studies have shown how inertia affects the unsteady propulsion of ciliated and larger swimmers [27–31]. The recent advancement of high-speed tunable microswimmers [32, 33] has brought this inertial regime into practical relevance, revealing opportunities for mass-dependent sorting of ABPs in flows. Beyond fundamental interest, particle separation based on mass in controlled environments opens up diverse applications, from selective particle sorting in microfluidics to effective filtration and the design of smart materials. For instance, in cancer research, the mass of cancer cells can be different from healthy ones, and this difference in mass can be used to identify and isolate cancer cells for further study [34]. Similarly, mass-based separation methods can detect and isolate specific proteins or pathogens in a sample associated with a specific disease. However, separation of entities based on their mass requires a predictive understanding of how particle mass, self-propulsion, and external flow influence each other to shape the particle trajectories in confined boundaries. Addressing these issues is the central aim of the present study. Earlier studies on the diffusion of microswimmers confirm that Poiseuille flows

^{*} ankitgupta@kgpian.iitkgp.ac.in

[†] Corresponding author: psburada@phy.iitkgp.ac.in

induce trajectory asymmetries, validating flow-driven manipulation approaches. Using the differential interaction of the particles with the flow field, it is possible to achieve separation. Importantly, while the segregation outcome manifests itself in distinct peak positions in particle velocity, these positions are not directly tunable through system parameters alone. Rather, our study highlights how the interplay of inertia and flow geometry establishes natural separation regimes, which can then be exploited for efficient and precise particle filtering in flat channels.

In this article, we study the diffusive behavior of ABPs in a microfluidic channel under the influence of external Poiseuille flow. By negating particle-wall interactions, we analyze how the mass of the particles and the self-propulsion speed determine the transport characteristics of ABPs. Previous works have identified swinging and tumbling regimes for rigid active particles in similar flows [13, 35], but the influence of inertia and mass heterogeneity on these regimes has not been explored. Our results reveal distinct migration behaviours tied to inertial effects, suggesting a mechanism of particles for selective transport and separation in microchannels. This article is organized as follows. In Sec. II, we introduce the model system of ABPs driven in a two-dimensional microfluidic channel under an externally imposed Poiseuille flow. The transport characteristics of ABPs are presented as a function of various system parameters in Sec. III. The discussion and the main conclusions are presented in Sec IV and Sec V, respectively.

II. MODEL

Consider the dynamics of an ABP of mass M suspended in a thermal bath and constrained to diffuse in a twodimensional (2D) flat channel subjected to a Poiseuille flow, as shown in Fig. 1. The particle self-propels in the direction of its orientation with a constant velocity $v_0 \hat{n}$, where $\hat{n} = (\cos \theta, \sin \theta)$ is the unit vector. Here, θ is the angle measured relative to the channel axis, i.e., x-axis. The Poiseuille flow u(y), which is directed along the x-axis and has a shear gradient along the y-axis with a local shear rate $\omega(y)$. Further, ABP may experience external rotation rate (chirality) Ω , where the sign of Ω defines the handedness.

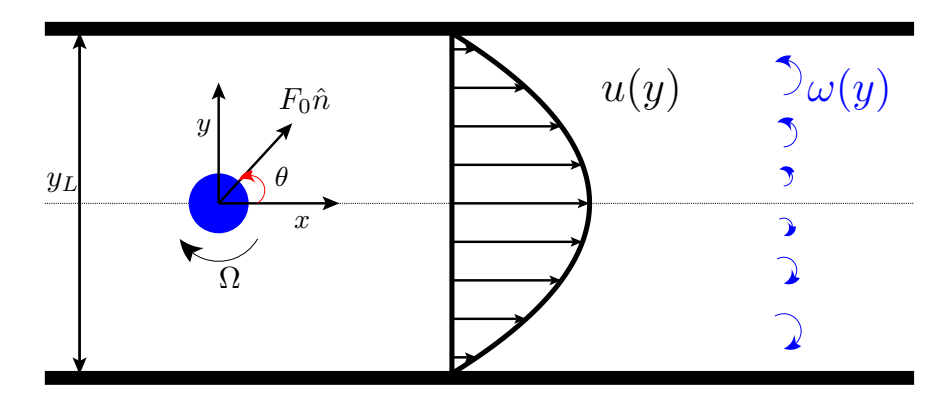


FIG. 1. Schematic of an ABP in a 2D microfluidic channel under a Poiseuille flow u(y). The particle is located at r=(x,y) and has a constant intrinsic speed in the direction of its orientation \hat{n} . The active force F_0 , self-propelled angle θ , chirality Ω , local shear rate $\omega(y)$, and width of the channel y_L are indicated.

The equation of motion of ABP is described by the Langevin equations as

$$M\frac{d^{2}\vec{r}}{dt^{2}} = -\gamma_{t}\frac{d\vec{r}}{dt} + F_{0}\hat{n} + \gamma_{t} u_{s}(y)\hat{x} + \sqrt{2D_{0}}\vec{\xi}(t)$$
(1)

$$\gamma_r \frac{d\theta}{dt} = \omega_s(y) + \Omega + \sqrt{2D_\theta} \chi(t), \qquad (2)$$

Eq. (1) and Eq. (2) govern the translational and rotational motion of ABP, where \vec{r} represents its position vector in 2D. $D_0 = (k_B T/\gamma_t)$ and $D_\theta = (k_B T/\gamma_r)$ are the translational and rotational diffusion constants, respectively. The self-propelled force $F_0 = \gamma_t v_0$. Here, k_B is the Boltzmann constant, and T is the temperature of the surrounding medium. γ_t and γ_r denote the translational and rotational friction coefficients, respectively. $\vec{\xi}(t)$ and $\chi(t)$ are zero-mean Gaussian white noises, which model the translational and rotational Brownian fluctuations due to the coupling of the particle with the surrounding medium, both obeying the fluctuation-dissipation relation $\langle \xi_i(t)\xi_j(t')\rangle = 2\delta_{ij} \delta(t-t')$ and $\langle \chi_i(t)\chi_j(t')\rangle = 2\delta_{ij} \delta(t-t')$ for i, j = x, y.

A 2D channel is described by two parallel walls with a separation distance y_L , see Fig. 1. The Poiseuille flow

imposed in this channel is prescribed as

$$u(y) = u_0 \left[1 - \left(\frac{2y}{y_L} \right)^2 \right],\tag{3}$$

where u_0 is the flow strength, and the corresponding local shear rate is calculated as

$$\omega(y) = -\frac{1}{2} \frac{du(y)}{dy} = \frac{4u_0 y}{y_L^2} \,, \tag{4}$$

which is depicted by the blue arrows in Fig. 1. Although the flow velocity decreases away from the centerline and vanishes at the channel walls $y = \pm y_L/2$, the local shear rate increases linearly with y, see Fig. 1. At the upper wall (y > 0), the local shear rate is in a counter-clockwise direction, and at the lower wall (y < 0), the local shear rate is in a clockwise direction. Due to the differential rotation arising from the asymmetric shear forces acting on the particles, the particles that are closer to the channel center are dragged more strongly by the flow compared to the particles near the wall.

In order to have a dimensionless description, we scale all length variables by the width of the channel y_L , i.e., $x \to x/y_L$ and $y \to y/y_L$. Similarly, we rescale the time as $t \to u_0 t/y_L$. With this, we can rescale the other parameters as $D_t \to D_0/(y_L u_0)$, $D_r \to y_L D_\theta/u_0$, and $\Omega \to y_L \Omega/u_0$. The dimensionless Langevin equation reads,

$$m\frac{d^2\vec{r}}{dt^2} = -\frac{d\vec{r}}{dt} + f_0\hat{n} + u(y)\,\hat{x} + \sqrt{2D_t}\,\vec{\xi}(t)$$
 (5)

$$\frac{d\theta}{dt} = \omega(y) + \Omega + \sqrt{2D_r} \chi(t), \qquad (6)$$

where the dimensionless mass reads $m = u_0 M/y_L \gamma_t$, $\tau_m = M/\eta_t$ is the time scale associated with the inertia of the particle. $f_0 = F_0/\gamma_t u_0$ is the dimensionless active force. In the rest of the paper, we use dimensionless variables. We assume that ABPs are point-sized entities without interacting with each other. By doing so, we can focus solely on the influence of confinement, self-propulsion, and inertial effects on single-particle dynamics, without the added complexity of collective behavior. Eqs. (5) & (6) are solved using the standard stochastic Euler algorithm over 2×10^4 trajectories with sliding boundary conditions at the channel walls [7, 36, 37]. Since particles along the y direction are confined, we calculate the average velocity $\langle v \rangle$ and the effective diffusion coefficient D_{eff} of the ensemble of ABPs along the channel direction (x direction), in the long-time limit, as

$$\langle v \rangle = \lim_{t \to \infty} \frac{\langle x(t) \rangle}{t} \,, \tag{7}$$

$$D_{eff} = \lim_{t \to \infty} \frac{\langle x^2(t) \rangle - \langle x(t) \rangle^2}{2t} \,. \tag{8}$$

III. TRANSPORT CHARACTERISTICS

In the absence of external forces or strong interaction between the particle and the walls, the steady-state distribution of the particle's position across the channel can be reasonably approximated as uniform. This approximation is valid when the particle's self-propulsion and rotational diffusion lead to a homogeneous exploration of the available space, and the channel width is not extremely narrow compared to the particle's persistence length. Under this assumption, the steady-state probability distribution for the particle position is

$$P(y) = 1, \quad -\frac{y_L}{2} \le y \le \frac{y_L}{2}.$$
 (9)

In this case, the average velocity of the particle in the x-direction can be obtained as

$$\langle v \rangle_{max} = \int_{-\frac{y_L}{2}}^{\frac{y_L}{2}} u(y) P(y) dy. \tag{10}$$

Thus, the maximum average velocity of the particles in the Poiseuille flow is

$$\langle v \rangle_{max} = \frac{2u_0}{3y_L}.\tag{11}$$

Note that if the particles accumulate near the channel boundaries due to inertia or some interaction, the distribution P(y) would no longer be uniform, and the average velocity could be less than this value. Further, this maximum value is the same for both passive and active particles.

A. Impact of particle mass

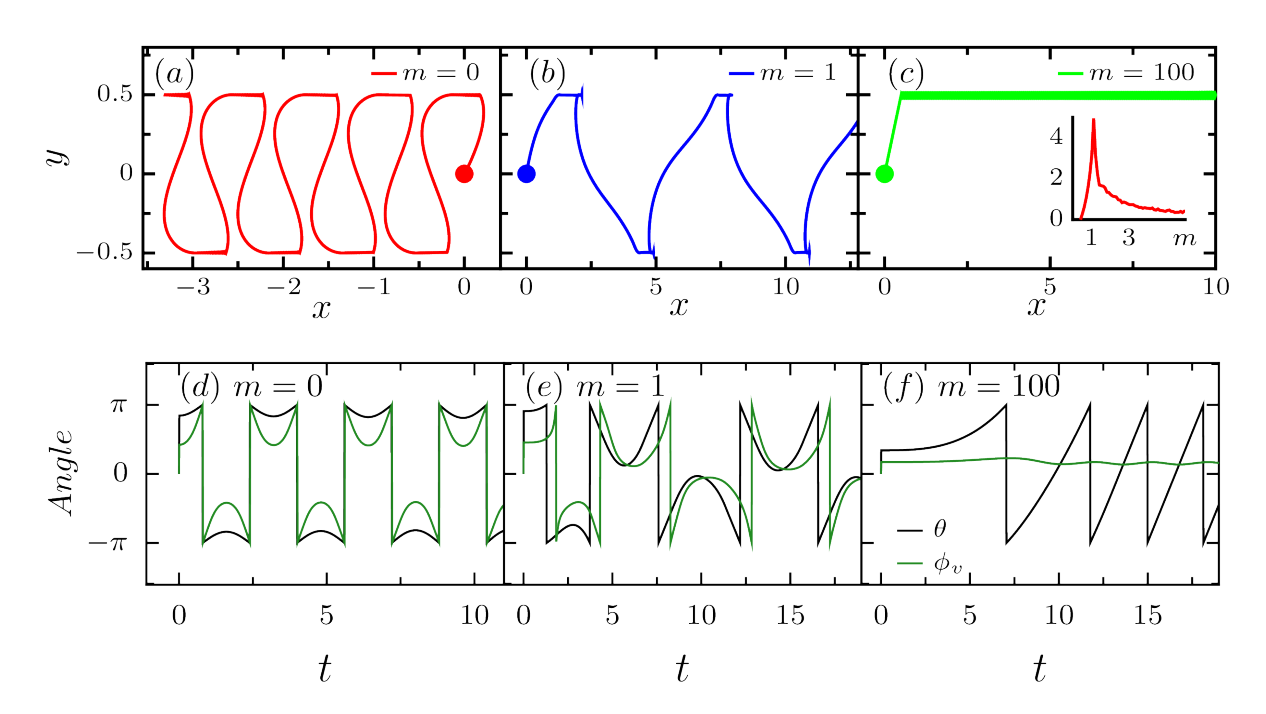


FIG. 2. (a)-(c) Deterministic trajectories of an active particle in a two-dimensional channel with a Poiseuille flow prescribed by Eq. (3). The particle starts at the center of the channel, i.e., x = y = 0, with different values of particle mass. (d)-(f) are the corresponding orientation $\theta(t)$ and the instantaneous velocity $\phi_v(t)$ directions. For $m \neq 0$, a lag develops between $\theta(t)$ and $\phi_v(t)$ due to the inertia of the particles. Trajectories are obtained by integrating Eq. (5) and Eq. (6) numerically for $D_t = D_r = 0$, $\Omega = 0$, and $f_0 = 1$.

To analyze the effect of the Poiseuille flow on inertial ABP dynamics, in Fig. 2, we show the deterministic trajectories of the particle confined in a two-dimensional channel under a Poiseuille flow, as described by Eqs. 5 & 6. In the overdamped regime (see panel (a)), the particle swims upstream the background flow, executing symmetric, channelspanning oscillations, a behavior driven by the interplay of self-propulsion and flow-induced reorientation. As inertia becomes significant (panel (b)), the particle trajectory transforms into a non-harmonic, asymmetric path, persistently biased downstream. The wavelength λ of the oscillatory trajectories increases with m, reaches a maximum around the optimum mass m_{op} , where the flow strength and mass are nearly equal. See the inset of Fig. 2(c). Further increase in m leads to particle accumulation near the channel boundaries [see inset in Fig. 2(c)] due to an increase in the inertia of particles. As a result, λ decreases. In the strongly underdamped regime (panel (c)), the particle ceases cross-channel oscillations entirely and instead self-propels along one of the side walls in a quasi-linear path, revealing a form of inertial wall-locking. This leads to a reduction in $\langle v \rangle$ (see Fig. 3). The panels (d)-(f) in Fig. 2 depict the corresponding temporal evolution of the orientation of the particle $\theta(t)$ and the angle of its instantaneous velocity direction $\phi_n(t)$. As the mass increases, a growing phase lag emerges between $\theta(t)$ and $\phi_n(t)$, highlighting the delay due to inertia of the particles [29] in the reorientation response of the particle to hydrodynamic shear (Eq. 4). Interestingly, these simulated trajectories closely mirror those observed in recent experiments on active Janus colloids and motile microswimmers in confined geometries under flow [26]. The emergence of upstream oscillatory motion, downstream drifting states, and wall-bound trajectories dependent on inertia suggests that our model captures essential features of active particle behaviors in microchannels.

The transport characteristics of ABPs are depicted in Fig. 3 for different values of $D=D_t=D_r$. In the overdamped regime $(m\to 0)$, the activity of the particles and the local shear rate lead to an upstream drift, evidenced by a negative average velocity $\langle v \rangle$, as shown in Fig. 3 and supported by Fig. 2(a). As m increases, $\langle v \rangle$ shows transitions from negative (upstream) to positive (downstream), marking a crossover point. Beyond this, $\langle v \rangle$ increases with m, and $\langle v \rangle$ becomes positive, i.e., currents in the positive x- axis of the channel, for different values of noise strength D. Around the critical value of mass $m\equiv 1$, the system enters an intermediate regime where both inertial and viscous forces are comparably influential. Here, particle inertia introduces a velocity relaxation timescale τ_m , which significantly affects transport behavior. The peak represents the optimal mass where particles can effectively utilize both their self-propelled motion and the favorable flow conditions. Since we considered $D=D_t=D_r$, the peak position is independent of D. However,

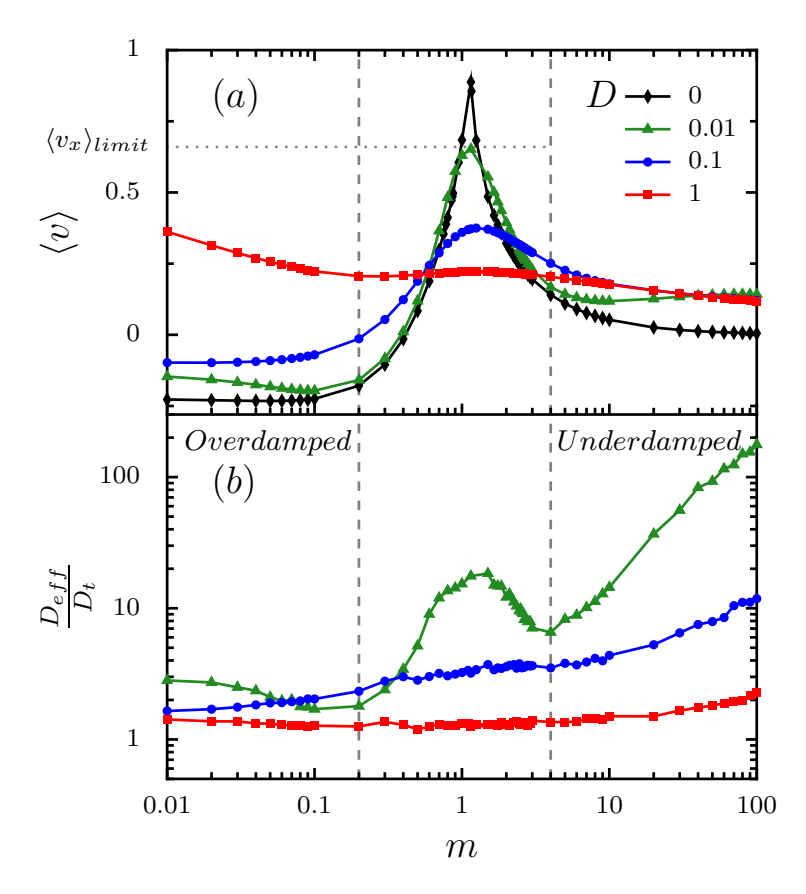


FIG. 3. (a) The average velocity $\langle v \rangle$ and (b) the effective diffusion coefficient D_{eff} as a function mass m of the particles for various values of the diffusion coefficient $D = D_r = D_t$. The horizontal dashed line indicates the maximum flow velocity in the channel, $\langle v_x \rangle_{limit}$ (Eq. (11)). The other parameters are set as, $\Omega = 0$ and $f_0 = 1$.

if $D_t \neq D_r$, there will be some shift in the peak position with a change in noise strength [see Fig. 5(a)&(c)]. Note that for the non-deterministic case, i.e., $D \neq 0$, $\langle v \rangle$ does not exceed the limit $\langle v_x \rangle_{limit}$ (Eq. (11)), which corresponds to the situation where particles are uniformly distributed along the transversal direction. On further increase in m, there is a gradual decay in $\langle v \rangle$ as the inertia of the particle becomes dominant. The effective diffusivity D_{eff} quantifies channel exploration rather than net drift. For D=0, D_{eff} is nearly zero since deterministic trajectories remain confined, and cannot be shown in the log-log plot.

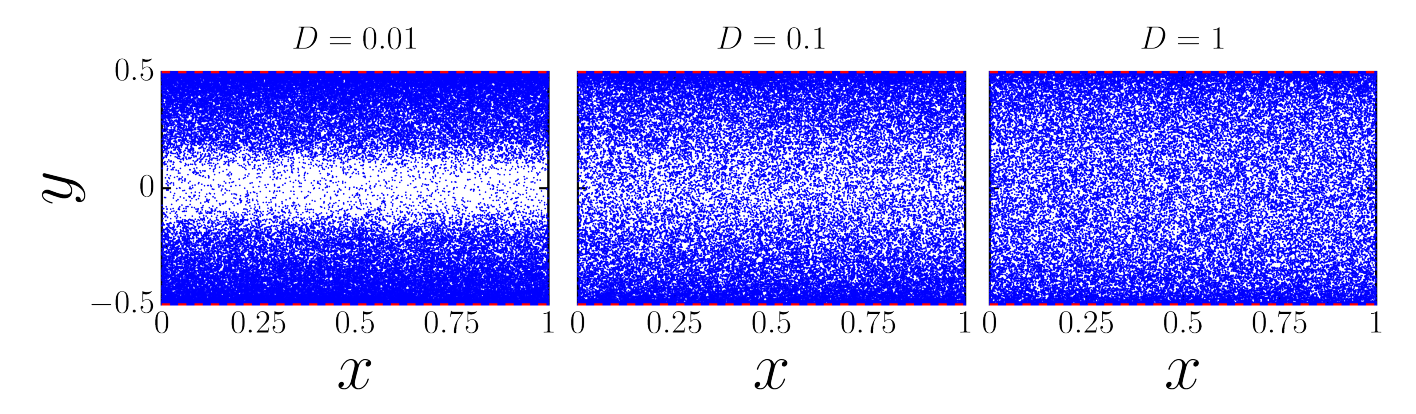


FIG. 4. The steady state distribution of chiral particles, for various values of the diffusion coefficient D. The other parameters are set as, m = 100, $u_0 = 1$, $\Omega = 0$ and $f_0 = 1$.

Introducing a weak noise (D = 0.01) produces a pronounced maximum in D_{eff} at an intermediate mass, where inertia extends orientational persistence while noise destabilizes periodic orbits. At larger noise strengths, dispersion

grows more broadly and $D_{\rm eff}$ increases monotonically with mass. In the higher mass regime, $\langle v \rangle$ is nearly independent of the noise strength D due to inertia, and particles exhibit a constant, low $\langle v \rangle$. Interestingly, in this regime, D_{eff} decreases with increasing D. For lower values of D, particles mostly accumulate near the channel boundaries and spread along the length of the channel (see Fig. 4). This leads to higher D_{eff} and lower $\langle v \rangle$. With an increase in D, particles tend to distribute all over the available space, leading to a uniform distribution along the traversal direction of the channel. Due to the external flow, all the particles tend to move together (with a lower $\langle v \rangle$), which leads to less spreading or lower D_{eff} . See Fig. 4.

B. Influence of translational and rotational diffusion constants

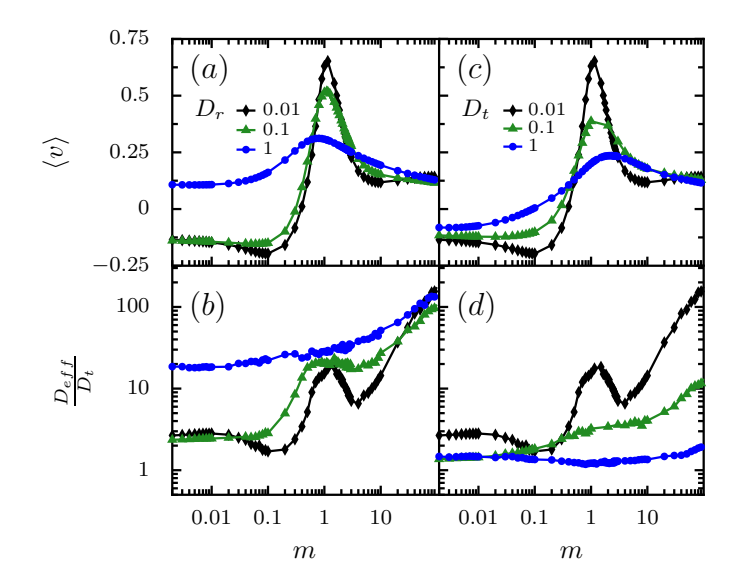


FIG. 5. (a) The average velocity $\langle v \rangle$ and (b) the effective diffusion coefficient D_{eff} as a function mass m for various values of the rotational diffusion coefficient D_r with $D_t = 0.01$. (c) The average velocity $\langle v \rangle$ and (d) the effective diffusion coefficient D_{eff} as a function of mass m for various values of the translational diffusion coefficient D_t with $D_r = 0.01$. The other parameters are set as, $\Omega = 0$ and $f_0 = 1$.

So far, we consider the case of $D=D_t=D_r$. Figure 5 illustrates the dependence of $\langle v \rangle$ and $D_{\rm eff}$ on particle mass m, for different values of translational diffusion D_t and rotational diffusion D_r . The observed trends can be attributed to the complex interplay between thermal noise, inertia, and shear-induced alignment. At lower values of D_r , due to the applied Poiseuille flow, local shear rate $\omega(y)$ aligns particles preferentially against the flow direction, leading to a suppression of $D_{\rm eff}$. In this regime, the orientation angle θ evolves slowly, enabling particles to maintain alignment upstream for extended durations and thus resulting in a net negative drift. As D_r increases, particle movement becomes more random, reducing the average alignment and consequently diminishing the upstream drift. This leads to a progressive decrease in the peak height of $\langle v \rangle$ and an increase in D_{eff} , particularly for particles with moderate mass, where inertial effects play a role but are not dominant.

On the other hand, translational diffusion D_t plays a relatively minor role in the overdamped regime but becomes increasingly significant in the intermediate and underdamped regimes. For moderate mass values, lower D_t preserves directional motion, resulting in a more pronounced peak in $\langle v \rangle$, whereas higher D_t introduces stronger translational noise that disrupts persistent motion and reduces $\langle v \rangle$. As observed before, particles having higher mass, $\langle v \rangle$ is nearly independent of both D_t and D_r . However, in this regime, D_{eff} reduces with increasing strength of D_t as discussed before in Fig. 3. Collectively, these results demonstrate that while rotational diffusion primarily controls alignment and drift in the $(m \to 0)$ limit, translational diffusion plays a vital role in the intermediate to underdamped regimes.

C. Effect of active force

Figure 6 (a) and (b) shows the dependence of $\langle v \rangle$ and D_{eff} on the particle mass m for various values of the self-propelled force f_0 respectively. It is evident that f_0 significantly modulates $\langle v \rangle$ especially in the overdamped regime. In this limit, increasing f_0 enhances the particle's ability to swim upstream against the background flow, resulting in

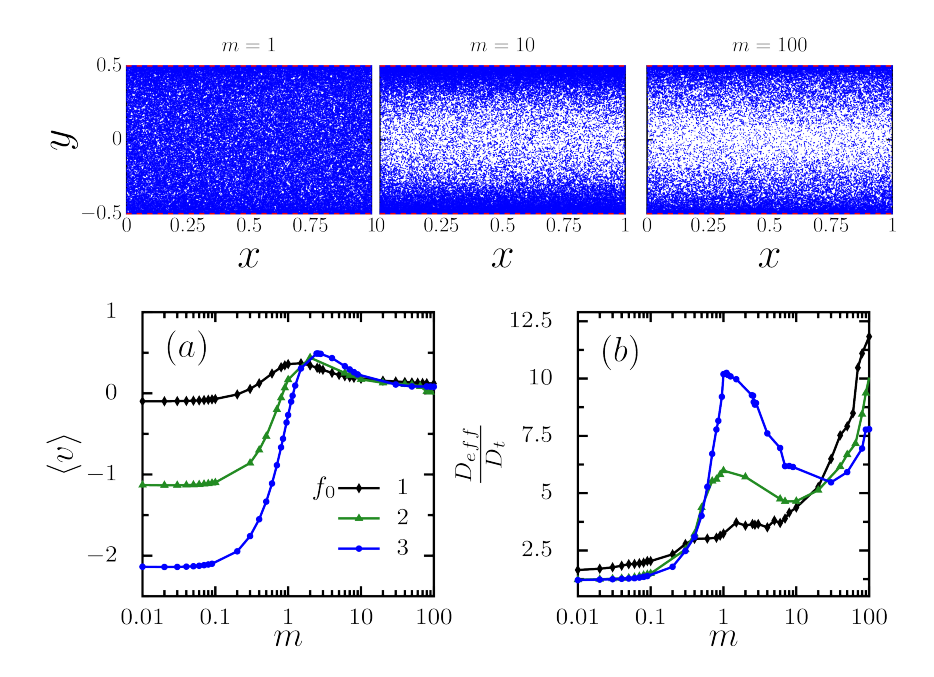


FIG. 6. (a) The average velocity $\langle v \rangle$ and (b) the effective diffusion coefficient D_{eff} as a function mass m for various values of active force f_0 . Additional parameters in the system are set as $D_r = D_t = 0.1$, and $\Omega = 0$. The top panel corresponds to the steady state distribution of active particles, for various values of the mass m, for $f_0 = 3$.

enhanced $\langle v \rangle$ in the negative x- direction. Since particles move together $|\langle v \rangle|$ is high and $D_{\rm eff}$ is low. As m increases, inertial effects begin to dominate, and the efficiency of upstream swimming is reduced. As observed before, around $m=1, \langle v \rangle$ becomes positive, indicating a transition to a downstream-dominated transport regime. The corresponding D_{eff} is increased monotonically, and the magnitude is greatly enhanced with the increase in f_0 . However, for higher f_0 , e.g., $f_0=3$, D_{eff} shows a non-montonic behavior for higher values of m. The latter can be understood with the help of the steady state distribution of ABPs for different values of m as depicted in the top panel of Fig. 6. For (m>1), the particles become increasingly entrained by the flow. As a result, $\langle v \rangle$ decays and D_{eff} slows down. In this regime, as observed before, particles start accumulating near the channel boundaries and spread along the channel length. In the limit of higher m, due to inertia $\langle v \rangle$ approaches zero. However, D_{eff} increases because of the noise effects and external flow.

D. Effect of external rotation rate

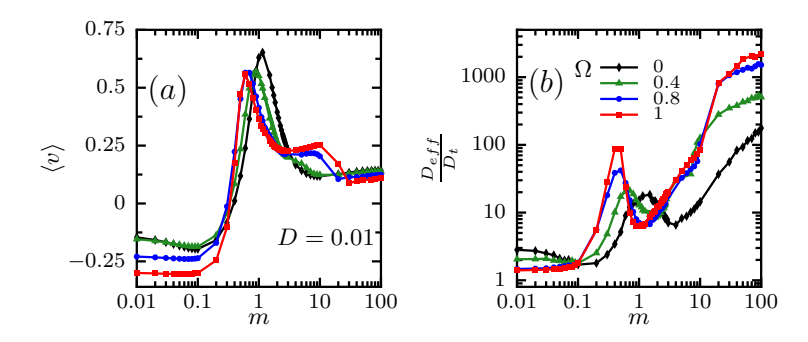


FIG. 7. (a) The average velocity $\langle v \rangle$ and (b) the effective diffusion coefficient D_{eff} as a function of mass m for various values of the rotation rate Ω . Additional parameters in the system are set as $D_r = D_t = 0.01$ and $f_0 = 1$.

Figure 7 (a) and (b) illustrates the behavior of $\langle v \rangle$ and D_{eff} on m for various values of the rotation rate Ω of the particles. The behaviors reveal that Ω significantly influences the dynamics of the particles. In the $m \to 0$ limit, at higher values of Ω , particles exhibit a stronger upstream drift, as reflected by increasingly negative values of $\langle v \rangle$.

This enhanced upstream motion indicates a more pronounced rotational activity that drives particles against the flow direction. Moreover, the peaks in both $\langle v \rangle$ and $D_{\rm eff}$ -which correspond to optimal drift and diffusion—shift toward lower mass values as Ω increases. This shift can be understood as a balance between persistence and inertia. When orientation changes rapidly at large Ω , only lighter particles with shorter inertial relaxation times can adapt effectively, shifting the optimum toward lower mass. For intermediate masses, where inertial and rotational timescales are comparable, inertia suppresses rapid reorientations without acceleration. This partial alignment between self-propulsion and rotational drift yields a modest enhancement in $\langle v \rangle$ and $D_{\rm eff}$. However, at higher mass values, $\langle v \rangle$ is independent of Ω but D_{eff} greatly enhances with Ω as the particles' rotational movement increases.

IV. DISCUSSION

The study of the inertial ABPs in a two-dimensional channel reveals a rich spectrum of transport behaviours arising from the interplay of mass, self-propulsion, and external flow. As observed in the overdamped limit, swimmers exhibit oscillatory upstream rheotaxis, characterized by periodic cross-channel motion against the flow, directly reminiscent of $E.\ coli$ and $T.\ brucei$ dynamics [38] and closely aligned with recent observations of droplets in confined flows [26]. This agreement validates the essential physics captured by our model and underscores its relevance for real and synthetic microswimmers. Accounting for inertia, the study uncovers qualitatively new regimes. Increasing particle mass weakens upstream motion, suppresses cross-stream oscillations, and promotes wall accumulation. The mean downstream velocity exhibits a non-monotonic dependence on mass, with an optimal m_{op} that maximizes drift speed; swimmers lighter or heavier than this optimum both drift more slowly.

To provide an estimate in real units, we consider a swimmer of radius $a \sim 1~\mu \text{m}$ in water at room temperature $(T \sim 300~\text{K})$. The translational friction coefficient is $\gamma \sim 2 \times 10^{-3}~\text{mg/s}$, with a rotational diffusion time $\tau_r \sim 50~\text{s}$. Typical propulsion speeds are $v_0 \sim 0.2~\mu \text{m/s}$. For a channel width $y_L = 10~\mu \text{m}$, the mapping yields an optimal effective mass $m^{op} \sim 0.1~\text{mg}$. Particles of this mass drift downstream with mean velocities $\sim 0.12~\mu \text{m/s}$. These predictions suggest that inertial rheotaxis can be exploited to design lab-on-chip devices for the selective guidance and separation of microswimmers, nanoparticles, and even cellular organelles based on mass.

V. CONCLUSION

In this study, we have numerically investigated the transport characteristics of non-interacting inertial active particles in a two-dimensional channel with a Poiseuille flow. Between the channel boundaries, active particles periodically accelerate, decelerate, and continuously change their swimming orientations. The transition from upstream to downstream motion of particles marks a fundamental change in active dynamics, arising when inertial effects become comparable to viscous forces. We have shown that inertia fundamentally reshapes microswimmer rheotaxis, e.g., the striking feature of upstream movement of ABPs in the over-damped regime and higher migration at optimal mass. We observed that as the mass of ABPs increases, they tend to accumulate near the channel walls and move along the channel boundaries due to the intrinsic nature of the particles and local shear rate due to the applied Poiseuille flow. As a result, particle velocity decreases and effective diffusion is greatly enhanced. These observed findings were further enhanced and controlled by the activity and chirality (rotation rate) of the particles as well as the temperature of the surrounding fluid. This establishes inertia as a key control parameter for guiding and separating active particles in confined flows, offering a passive route to mass-selective transport. This study provides design principles for microfluidic technologies and invites extension to 3D geometries and hydrodynamic interactions, advancing predictive control of active matter.

VI. ACKNOWLEDGMENT

This work was financially supported by SERB, Government of India, project-wide CRG/2023/006186. The authors acknowledge the Indian Institute of Technology (IIT) Kharagpur for providing research facilities.

^[1] S. Ramaswamy, Annual Review of Condensed Matter Physics 1, 323 (2010).

^[2] E. Lauga and T. R. Powers, Reports on Progress in Physics 72, 096601 (2009).

- [3] M. C. Marchetti, J. F. Joanny, S. Ramaswamy, T. B. Liverpool, J. Prost, M. Rao, and R. A. Simha, Reviews of Modern Physics 85, 1143 (2013).
- [4] J. Elgeti, R. G. Winkler, and G. Gompper, Reports on Progress in Physics 78, 056601 (2015).
- [5] C. Bechinger, R. Di Leonardo, H. Löwen, C. Reichhardt, G. Volpe, and G. Volpe, Reviews of Modern Physics 88, 045006 (2016).
- [6] Z. Peng and J. F. Brady, Physical Review Fluids 5, 073102 (2020).
- [7] N. Khatri and P. S. Burada, Physical Review E 105, 024604 (2022).
- [8] P. Galajda, J. Keymer, P. Chaikin, and R. Austin, Journal of Bacteriology 189, 8704 (2007).
- [9] J. Schwarz-Linek, C. Valeriani, A. Cacciuto, M. E. Cates, D. Marenduzzo, A. N. Morozov, and W. C. K. Poon, Proceedings of the National Academy of Sciences 109, 4052 (2012).
- [10] C. Villalobos-Concha, Z. Liu, G. Ramos, M. Goral, A. Lindner, T. López-León, E. Clément, R. Soto, and M. L. Cordero, Proceedings of the National Academy of Sciences 122, 10.1073/pnas.2426096122 (2025).
- [11] J. Palacci, S. Sacanna, S.-H. Kim, G.-R. Yi, D. J. Pine, and P. M. Chaikin, Philosophical Transactions of the Royal Society A: Mathematical, Physical and Engineering Sciences 372, 20130372 (2014).
- [12] S. van Kesteren, L. Alvarez, S. Arrese-Igor, A. Alegria, and L. Isa, Proceedings of the National Academy of Sciences 120, 10.1073/pnas.2213481120 (2023).
- [13] A. Zöttl and H. Stark, Physical Review Letters 108, 218104 (2012).
- [14] R. Levy, D. B. Hill, M. G. Forest, and J. B. Grotberg, Integrative and Comparative Biology 54, 985 (2014).
- [15] T. Bhattacharjee and S. S. Datta, Nature Communications 10, 10.1038/s41467-019-10115-1 (2019).
- [16] J. Rutllant, M. López-Béjar, and F. López-Gatius, Reproduction in Domestic Animals 40, 79 (2005).
- [17] M. Engstler, T. Pfohl, S. Herminghaus, M. Boshart, G. Wiegertjes, N. Heddergott, and P. Overath, Cell 131, 505 (2007).
- [18] X. Ma, K. Hahn, and S. Sanchez, Journal of the American Chemical Society 137, 4976 (2015).
- [19] L. Soler and S. Sánchez, Nanoscale 6, 7175 (2014).
- [20] W. Gao and J. Wang, ACS Nano 8, 3170 (2014).
- [21] D. Reguera, A. Luque, P. S. Burada, G. Schmid, J. M. Rubí, and P. Hänggi, Phys. Rev. Lett. 108, 020604 (2012).
- [22] P. S. Burada, Y. Li, W. Riefler, and G. Schmid, Chemical Physics 375, 514 (2010).
- [23] C. Jin, S. M. McFaul, S. P. Duffy, X. Deng, P. Tavassoli, P. C. Black, and H. Ma, Lab Chip 14, 32 (2014).
- [24] J. Elgeti and G. Gompper, EPL (Europhysics Letters) 101, 48003 (2013).
- [25] R. Rusconi, J. S. Guasto, and R. Stocker, Nature Physics 10, 212 (2014).
- [26] R. Dey, C. M. Buness, B. V. Hokmabad, C. Jin, and C. C. Maass, Nature Communications 13, 10.1038/s41467-022-30611-1 (2022).
- [27] S. Wang and A. Ardekani, Physics of Fluids **24**, 10.1063/1.4758304 (2012).
- [28] L. Ren, D. Zhou, Z. Mao, P. Xu, T. J. Huang, and T. E. Mallouk, ACS Nano 11, 10591 (2017).
- [29] C. Scholz, S. Jahanshahi, A. Ldov, and H. Löwen, Nature Communications 9, 10.1038/s41467-018-07596-x (2018).
- [30] H. Löwen, The Journal of Chemical Physics 152, 10.1063/1.5134455 (2020).
- [31] R. Maity and P. Burada, Journal of Fluid Mechanics 940, 10.1017/jfm.2022.239 (2022).
- [32] Y. Kim and X. Zhao, Chemical Reviews **122**, 5317 (2022).
- [33] A. Aghakhani, O. Yasa, P. Wrede, and M. Sitti, Proceedings of the National Academy of Sciences 117, 3469 (2020).
- [34] S. Suresh, Acta Materialia **55**, 3989 (2007).
- [35] A. Zöttl and H. Stark, The European Physical Journal E 36, 10.1140/epje/i2013-13004-5 (2013).
- [36] A. Gupta and P. S. Burada, Physical Review E 108, 034605 (2023).
- [37] X. Ao, P. Ghosh, Y. Li, G. Schmid, P. Hänggi, and F. Marchesoni, The European Physical Journal Special Topics 223, 3227 (2014).
- [38] N. Heddergott, T. Krüger, S. B. Babu, A. Wei, E. Stellamanns, S. Uppaluri, T. Pfohl, H. Stark, and M. Engstler, PLoS Pathogens 8, e1003023 (2012).